ORIGINAL ARTICLE

Study of Wall Static Pressure Distribution on Flat Surface by Impinging Submerged Jet from Non-circular Orifice

A.M. Hanchinal[1*], R.N. Patil[2] and V.V. Katti[2]

[1]Department of Mechanical Engineering, Jain CET, Hubballi, India-580031
Phone: +91-9740169907
[2]Department of Mechanical Engineering, KLS VDIT, Haliyal, India-581329

ABSTRACT – The distribution of wall static and stagnation (CP and CP_O) pressure coefficient on a flat rectangular element by impinging air jet from the hexagonal orifice is obtained from experimentation. The past research studies helped to identify key parameters such as orifice geometry, jet exit-to-plate-distance (Z/d_j), test section inclination (θ), jet Reynold number (Re), lateral distance-to-jet diameter (X/d_j), test surface type and geometry, for better and acceptable results. The experimental outcome helps to know the effect of identified key parameters on wall static and stagnation pressure on a rectangular test plate in a confined flow path. The independent nature of wall static pressure is observed for all jet Reynold number ($10000 \leq Re \leq 50000$). Higher pressure coefficient values were observed at lower $Z/d_j = 1$, $X/d_j = 0$ and $\theta = 0$. A significant drop in CP values are seen with the increase in Z/d_j, X/d_j and θ. The experimental CP and CP_O contribution of confined flow are compared against the unconfined flow, around 48% to 58% enhancement is observed when confinement is used. Experimental pressure drop measurements across orifice were made and pressure loss coefficient (P_C) for hexagonal orifice of confined and unconfined condition are reported.

NOMENCLATURE

d_e	equivalent diameter of orifice	mm
d_j	hydraulic diameter of orifice	mm
m_a	mass flow rate of air	kg/s
Z	distance between test surface plane and orifice exit plane	mm
X	lateral distance of jet	mm
V_j	jet velocity at orifice exit	m/s
ρ_a	density of atmospheric air	kg/m^3
ρ_j	density of air at orifice exit	kg/m^3
μ	absolute viscosity of air	kg/ms
θ	inclination angle	°
v	voltmeter reading	mv
P_a	atmospheric pressure	N/m^2
T_j	jet temperature at exit	°C
C_d	co-efficient of discharge	
CP	static pressure coefficient	
CP_O	stagnation pressure coefficient	
P_C	pressure loss coefficient	
Re	jet Reynold number	
Z/d_j	dimensional less distance between orifice exit and rectangular test surface	
X/d_j	dimensional less axial position of orifice	

INTRODUCTION

Impinging jet is the most effective and active approach in thermal management (heating or cooling). As a result, it has many industrial applications such as, in the continuous casting of iron rods, annealing, food processing, and cooling of heated rotary cylindrical kilns of in the cement industries [1-4]. In jet impingement method the working fluid flows in the desired channel which accelerates the jet to high velocity when it is coming out from nozzles or orifice of a particular design. Due to its better and acceptable results, jet impingent method extended its area into various thermal applications. The effectiveness of impinging jet is influenced by the dimensional and non-dimensional parameters which are outlined in many best articles from researchers. In this approach, numerous experimental and numerical studies are carried out to

understand the behaviour of jet on different test surfaces configurations and come up with valuable and an acceptable results in the fluid of thermal science which help in the design and modifications of impinging jet applications [5-8].

The early studies considered a conventional circular jet but in the recent studies focused on the analysis of non-circular jet in both open and confined flow. The observation on jet impingement strategies with non-circular jets has grown in top-notch fee, and early research involves open flow impingement condition. The results from these studies are considered as the base for many research studies till now [9-10]. In 2011, Kanamori et al. [11] studied flow and heat transfer behaviour along with flow visualisation using hydrogen bulbs, Cu-Co thermocouples and CCD camera by impinging an air jet on a flat plate with polygon orifice having 3 to 6 sides. The results show at lower Z/d_j the impinging pattern on the test section takes the same profile as of orifice shape and higher Z/d_j these profile changes to circular shapes. Later in 2015 experimental and numerical study by Singh et al. [12] to identify the Z/d_j (4 to16) effect on Nusselt number (Nu) and CP distribution by impinging jet from a different nozzle on convexly curved cylinder for jet Re = 10000 to 25000 and correlations are obtained for stagnation Nu. In 2016 Trinh et al. [13] used FLIR titanium IR camera and RMS Numerical module and they observed the development of shear layer between jet and orifice configurations, a parabolic and non-parabolic profile for velocity are seen due to vena contraction effect. In 2016 Reodikar et al. [14] carried experiment using IR technique and compared results of heat transfer for circular and non-circular orifices, and they observed better Mach number for non-circular orifice under the same flow condition. In 2016 Meena et al. [15] carried heat transfer study using IR camera technique and observed maximum Nusselt number distribution (Nu) for Z/d_j =4 on impinging square, triangular, elliptical and circular jet on a flat surface, axis switch takes at 45º, 180º and 90º respectively. In the above-discussed studies, most of the research results give the effect of jet to test plate section distance for unconfined flow.

In 2017 Guo et al. [16] used digital particle image velocimetry method to analyse jet vertex phenomena for confined flow. In 2017 Attalla [17] used a square jet to study the uniformity of heat transfer on a flat surface and the results show 10.7% better uniformity in heat transfer when compared to the circular jet. In 2017 Muvvala et al. [18] carried experimental study to understand the fluid flow and heat distribution on a flat plate by impinging jet from a square nozzle (perforated nozzles). In 2018 the elliptical jet behaviour and vertical structures on a convex surface were identified by Long and New [19], and the results of convex surface are compared with the results of a flat surface. Abraham and Vedula [20] identified the effectiveness distribution on a convex element using a row of a single jet for different inclination, and the results show a decrease in the effectiveness with an increase in the inclination of the jet. In 2018 the use temperature-sensitive paint and particle image velocimetry method gave good results with a lobed nozzle compared with a circular nozzle by He and Liu [21]. In 2019 an experimental study carried by Singh and Prasad [22] shows 8-24% better result in the thermal performance factor for 45º chamfered exit and also the outlined correlations for average Nusselt number. Hanchinal and Katti [23] used four different orifice geometries to analyse the distribution of CP and CPo on test surface. The study shows better results for circular jet when compared to square, rectangular and triangular jet. In 2020 Patil et al. [24] studied the effect confined spent air on wall pressure distribution; the study shows better results for one side exit of air. Hanchinal and Katti [25] carried an experimental study on a convex surface using a coaxial jet for the confined and unconfined conditions. The results show a higher value of wall static pressure for the confined condition.

From the literature, it can be figured that most of the works are related to heat transfer distribution, and few studies are associated with the in-depth study on pressure distribution for the confined condition. Thus, in the present work, the attention is given to investigate experimentally the distribution of wall static pressure, CP and CPo, by impinging a non-circular air-jet on a rectangular element for both confined and unconfined flow to understand the effect of non-circular orifice and confinement on wall static pressure.

EXPERIMENTATION AND METHODOLOGY

The schematic representation for the present experimental work is shown in Figure 1. The air blower of 11500 rpm with a discharge capacity 2.9 m³/min and pressure head of 600 mm of water at atmospheric condition is used as a primary source of air for impingement of jet through a proposed orifice configuration. Based on the literature study, a 275 mm × 50 mm × 10 mm flat smooth rectangular transparent acrylic element is considered as a test surface. A calibrated valve controller used to adjust free air coming from the blower is made to impinge on the test element through an orifice for confined and unconfined flow. The dimensionless Reynold number (Re) of the jet is obtained from venturi meter whose coefficient of discharge, C_d is ± 0.92. The air at specified jet Reynold number is allowed to impinge on the test surface. From the literature study, it is noticed to most of the early studies considered conventional circular, square, triangular, rectangular, lobed shaped exit for jet (nozzles or orifice). The hexagonal orifice geometry has not been widely studied so far; thus a specific hexagonal orifice is prepared and used in the present study. Figure 2 shows the hexagon orifice and the design configuration for the hexagonal orifice as given in Table 1. The effective impingement of jet is observed when the jet flow is fully developed. For completely developed flow at jet exit length of a pipe taken 100 times the hydraulic diameter of a jet (d_j) and nozzle length-to-diameter ratio of 83 is taken [3] but in the present study the jet exit is from orifice type hence the length to diameter ratio is not considered.

1. Manometer to measure CP and CP_O, 2. Pitot tube, 3. Test element, 4. Confinement, 5. Orifice, 6. Tube,
7. Venturi meter, 8. Manometer to measure Re, 9. Pressure indicator,10. Control valve, 11. Pressure regulator,
12. Air blower, 13. Flexible pipe.
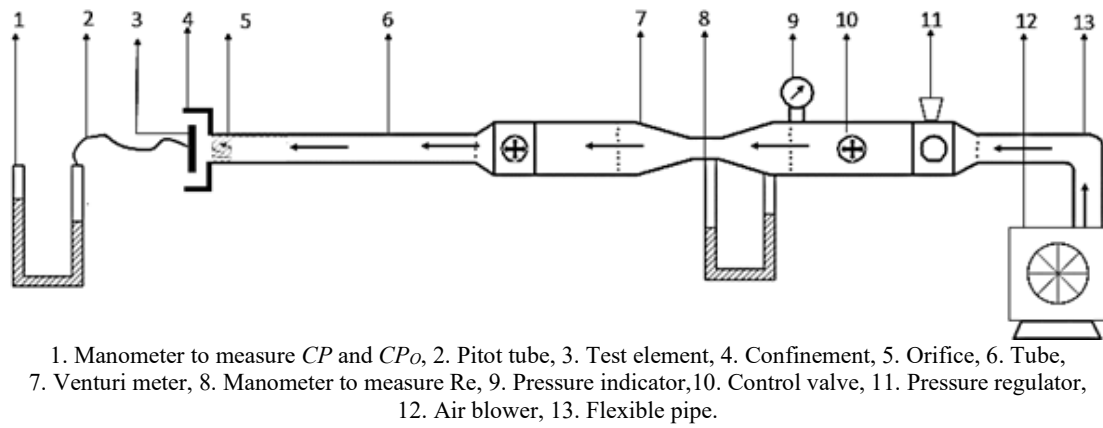
Figure 1. Schematic representation of experimental setup.
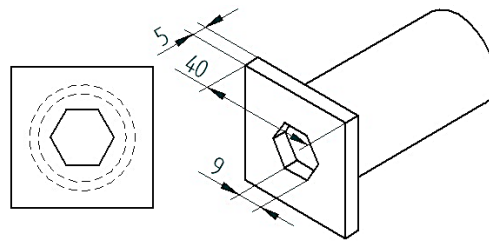
Figure 2. Design configuration of the non-circular orifice (all dimensions are in mm).

Table 1. Detail specification of the orifice.

Type of orifice	Side (mm)	Area (mm²)	Equivalent diameter, d_e (mm)	Hydraulic diameter, d_j (mm)
	9	210.44	18.47	15.6

A calibrated two-axis adjustable table with the least count of 0.05 mm is used to maintain test surface positions at various Z/d_j (1 to 5) and X/d_j (0 to 5). The CP and CPo on a rectangular test element is identified using a pressure tap (Probe of 0.5mm diameter) attached to the test plate without disturbing the surface and flow field of the jet. The jet temperature is identified by using a k-type thermocouple, and the calibration of the thermocouple is done with the help of RTD where the relation is obtained as $T_j = 22.168 \times v + 2.902$. A free movement is given to the rectangular test plate using sliders at both ends of the test surface so that CP can be measured at various test plate inclinations (0° to 40°). A 5 mm thick acrylic sheet is used to create a half-cut duct of size 70 mm × 80 mm × 250 mm. This duct is used to create a confinement effect on a test surface; this confinement duct guides impinged air to flow out in a well-defined path after impinging on a rectangular test surface as shown in Figure 3. The air is allowed to impinge on the plate through an orifice (hexagon) at a particular Reynold number. Once the study state reached, the wall static pressures were measured at a various flow and geometric parameters mentioned in Table 2. The wall pressure values are noted at various configurations using a long U-tube manometer, and the pressure values are in terms of mm of water deflection. The obtained values from manometers are substituted in a simplified static pressure equation to get particular wall pressures. All the experimental data are tabulated, and different x-y plots are drawn to obtain experimental CP and CP_O values for further analysis. The same experimental procedure is adopted to identify the experimental CP and CP_O values for unconfined condition.

Table 2. Parameters considered in the study.

Test element	Re	(θ)	(Z/d_j)	(X/d_j)	Flow type
Flat Rectangular	10000 to 50000	0° to 40°	1 to 5	0 to 5	Confined & unconfined

Data Reduction

During experimentation, the pressure values were obtained with the help of a sensitive manometer. The following are some of the important equations considered in the calculation of CP values at various conditions, and these equations are formed with reference from the literature [24-26].

The jet Reynolds number is a very important parameter that describes whether the jet is laminar or turbulent, in the present experimental study, the jet Reynold number is calculated using Eq. (1).

$$Re = \frac{4 \times \dot{m_a}}{\pi \times d_e \times \mu} \tag{1}$$
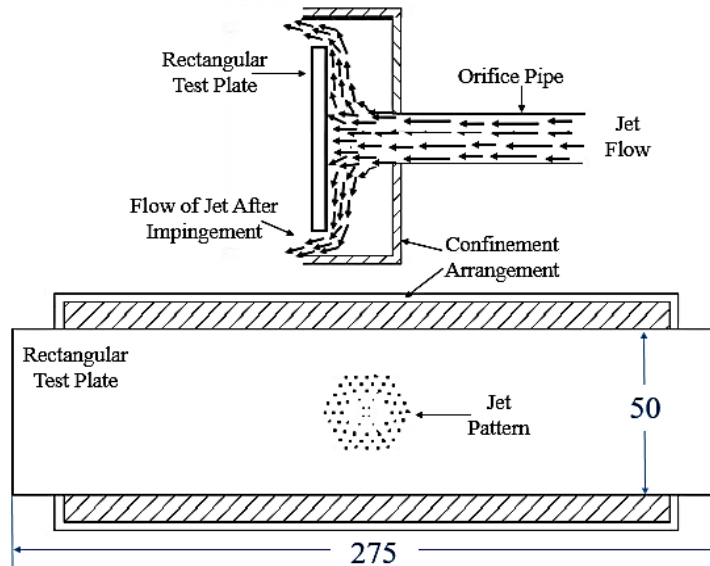
Figure 3. Schematic representation flow of jet (all dimensions are in mm).

The jet temperature is calculated using k-type thermocouple; Eq. (2) is the thermocouple relation which helps to identify the exact jet temperature. The jet temperature measured is used to identify the density jet (air) using Eq. (3).

$$T_j = 22.168 \times v + 2.902 \tag{2}$$

$$\rho_j = \frac{P_a}{0.287 \times (T_j + 273)} \tag{3}$$

The wall pressure is greatly influenced by jet velocity; thus, the jet velocity is identified using Eq. (4).

$$v_j = \frac{4 \times m_a}{\pi \times d_j \times \rho_j} \tag{4}$$

Once the jet velocity, density is identified the wall static pressures are calculated for all flow and geometric properties using Eq. (5). ΔP is a pressure difference between the impinging surface and atmosphere.

$$CP = \frac{\Delta P}{\frac{1}{2} \times \rho_a \times v_j^2} \tag{5}$$

The instrument calibrations are made for standard, and acceptable results and respective uncertainty in the primary quantities are calculated, for calculation the ISO guide is referred [28] along with Moffat [29] and Kline and McClintock [30] methods, which are adapted to identify the uncertainty of derived quantities. Based on the maximum measuring value, the uncertainties are identified. The uncertainty of the pressure tap probe is ±0.6 % FS. For orifice/venturi metre the uncertainty of C_d is ±3 %. For jet temperature, the uncertainty of k-type thermocouple is ±0.8 % and for power supply is ±1.9%. In the present study, the average value of uncertainty in pressure measurement is 4.5 %, respectively at jet Re of 10000 and 50000. The uncertainty analysis in the present study is based on the Moffat [29] method. The uncertainty in the estimation of C_d can be computed using Eq. (6).

$$\frac{\delta C_d}{C_d} = \left[\left(\frac{\delta l}{l}\right)^2 + \left(\frac{\delta b}{b}\right)^2 + \left(\frac{\delta h}{h}\right)^2 + \left(\frac{\delta t}{t}\right)^2 + \left(\frac{\delta A_o}{A_o}\right)^2 + 0.25 \left(\frac{\delta \Delta P}{\Delta P}\right)^2 + 4 \left(\frac{\delta \beta}{\beta}\right)^2 \right]^{0.5} \tag{6}$$

$$\frac{\delta C_d}{C_d} = \left[\left(\frac{1}{490}\right)^2 + \left(\frac{1}{320}\right)^2 + \left(\frac{1}{150}\right)^2 + \left(\frac{0.01}{270.65}\right)^2 + (0.0125)^2 + 0.25 \left(\frac{1}{49}\right)^2 + 4(0.0074)^2 \right]^{0.5} = 0.0232$$

Similarly, uncertainty in the computation of Reynolds number is done using Eq. (7) and also a sample calculation is shown.

$$\frac{\delta Re}{Re = \left[\left(\frac{\delta \dot{m}}{\dot{m}}\right)^2 + \left(\frac{\delta d}{d}\right)^2\right]^{0.5}}$$

$$\frac{\delta Re}{Re = \left[(0.03185)^2 + \left(\frac{0.1}{15.5}\right)^2\right]^{0.5}} = 0.03249$$

(7)

A sample uncertainty calculation in estimation of wall static pressure coefficient is as shown in Eq. (8).

$$\frac{\delta C_P}{C_P} = \left[\left(\frac{\delta \Delta P}{\Delta P}\right)^2 + \left(\frac{\delta V_j}{V_j}\right)^2\right]^{0.5}$$

$$\frac{\delta C_P}{C_P} = [(0.0055)^2 + (0.032)^2]^{0.5} = 0.06423$$

(8)

The uncertainty analysis for other measuring quantities was computed with a similar procedure by referring to the Moffat [29] method.

RESULTS AND DISCUSSION

The measurement of CP and CPo by impinging an air jet from non-circular (hexagon) orifice on a rectangular element is experimentally studied with high precision under the study state condition. Various x-y plots are drawn for the results, which are discussed in details for concluding the present study.

Influence of Jet Reynolds Number on Wall Static Pressure

The laminar and turbulent nature of the fluid flow is identified by a non-dimensional parameter Reynolds number. In the present study, an experiment is carried for turbulent flow (of Re = 10000-50000). Figure 4 and Figure 5 show the CP distribution at various test section angle (θ = 0° to 40°) for Z/d_j = 1 to 4 and X/d_j = 1. The graph of CP vs θ shows the independent characteristic of jet Re on the distribution of non-dimensional CP and CP_O value for all Z/d_j = 1 to 5 in both confined and unconfined flow condition, as all the curves take same profile for all jet Re (50000-10000) with some minor deflection in CP magnitude. Similar independency of jet Reynolds nd CPo was observed and highlighted in most studies [23-25]. It is also observed that the CP and CPo are dependent on flow restriction and non-dimensional jet exit distance (Z/d_j) and lateral distance (X/d_j) which are discussed in other sections.

(a) CP vs θ at Z/d_j = 1 and X/d_j = 1   (b) CP vs θ at Z/d_j = 2 and X/d_j = 1
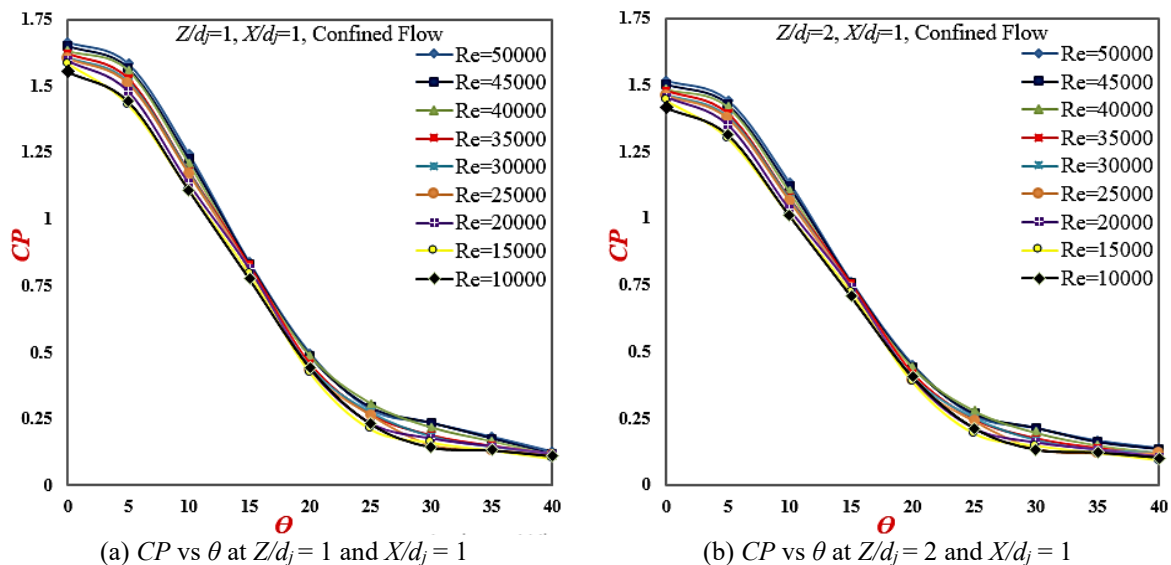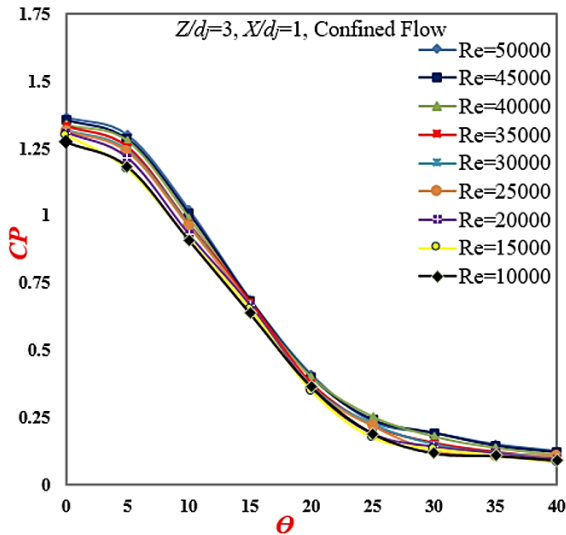
(c) CP vs θ at $Z/d_j = 3$ and $X/d_j = 1$.
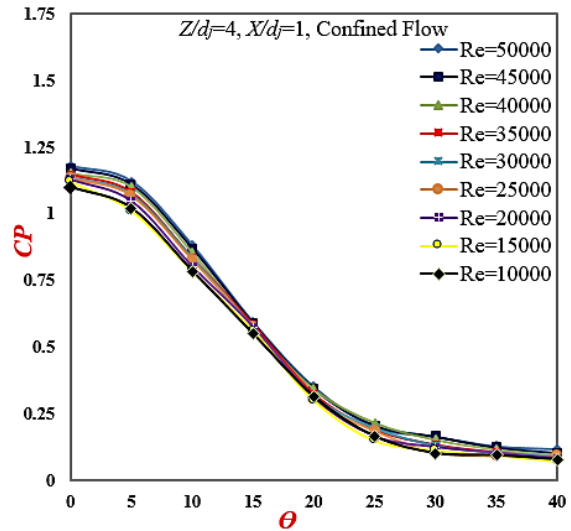
(d) CP vs θ at $Z/d_j = 4$ and $X/d_j = 1$.

Figure 4. Variation of wall pressure coefficient along with the test element inclination for confined flow.

Influence of Test Plate Inclination on Pressure Coefficient.

Test plate angle or inclination (θ) is a key parameter that influences the CP and CPo distribution on any element. From Figure 6, it is observed that the pressure coefficient magnitude changes with change in θ and similar changes are noted for unconfined flow. It is known that the jet velocity is maximum at the centre of the jet when θ changes ($\theta > 0^o$) the stagnation streamline of jet drifts from the centreline of the rectangular test plate which leads to expansion of the sub-atmospheric region in circumferential location. As a result, CP drops to a lower value, and the higher values of CPo are identified at $\theta = 0^o$. When $\theta = 0°$ jet is more effective as the maximum velocity of jet impinges on the rectangular test plate, which leads jet to get maximum dynamic pressure; as a result, CP reaches a peak value at $\theta = 0^o$ compared adjacent θ on the test element. Thus, when θ varied between $0°$ and 12° around 16% to 21% and when θ is between $13°$ to 40° around 31% to 43%, drop in the CP are noted for both confined and unconfined condition. Therefore for smaller test section inclination, higher CP values are observed for all examined flow parameters. Similar contributions are highlighted in early experimental studies [24-26]. Figure 8 shows a variation of CP along the axial or lateral position of the rectangular plate for $Z/d_j = 1$ to 4 at $Re = 40000$.

(a) CP vs θ at $Z/d_j = 1$ and $X/d_j = 1$

(b) CP vs θ at $Z/d_j = 2$ and $X/d_j = 1$.

(c) CP vs θ at $Z/d_j = 3$ and $X/d_j = 1$.
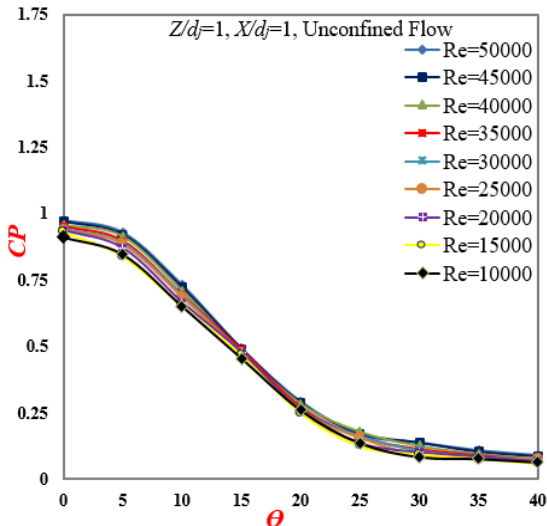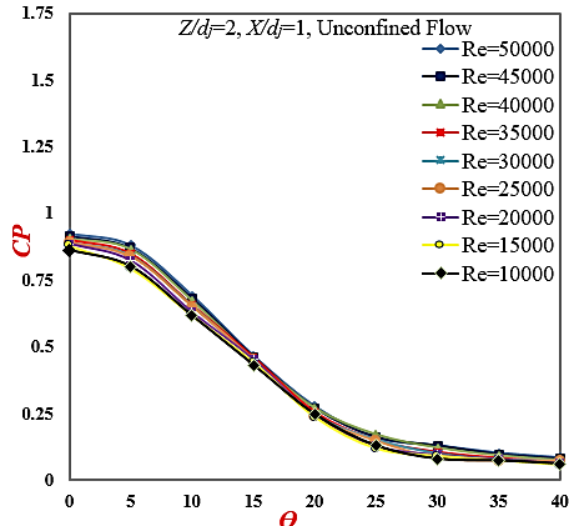
(d) CP vs θ at $Z/d_j = 4$ and $X/d_j = 1$.
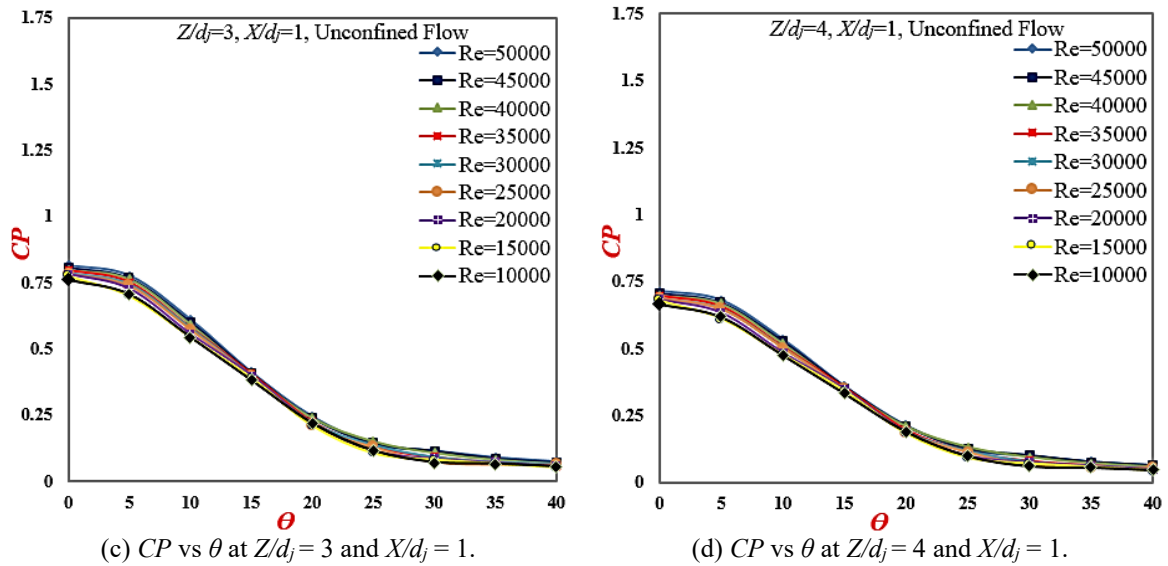
Figure 5. Variation of pressure coefficient along the test element inclination for unconfined flow.

Influence of Orifice Exit-to-test Plate on Pressure Coefficient

The variation of CP and CPo is greatly influenced by the orifice exit-to-test plate(Z/d_j) and lateral or axial position (X/d_j) of the jet. From Figure 6 and Figure 7, it is observed that as the Z/d_j value increases the CP and CPo magnitude drops to a lower value, that is at $Z/d_j = 4$, the low magnitude of CP and CPo are identified for all examined Re. With an increase in the Z/d_j around 32% to 37%, drop in the CP and CPo is observed. As the Z/d_j increases, a significant drop in the jet velocity is observed due to the spreading of the jet, which leads to a reduction in the jet strength by reducing the kinetic energy of jet. This spreading of the jet is observed from the flow visualisation method [26]. The same trend is observed for both confined and unconfined flow. Therefore from this analysis, it is understood that for smaller Z/d_j higher CP and CPo values are observed for all examined flow parameters, and similar experimental outcomes are seen in early studies [25-27].

(a) CP vs θ for confined flow

(b) CP vs θ for unconfined flow
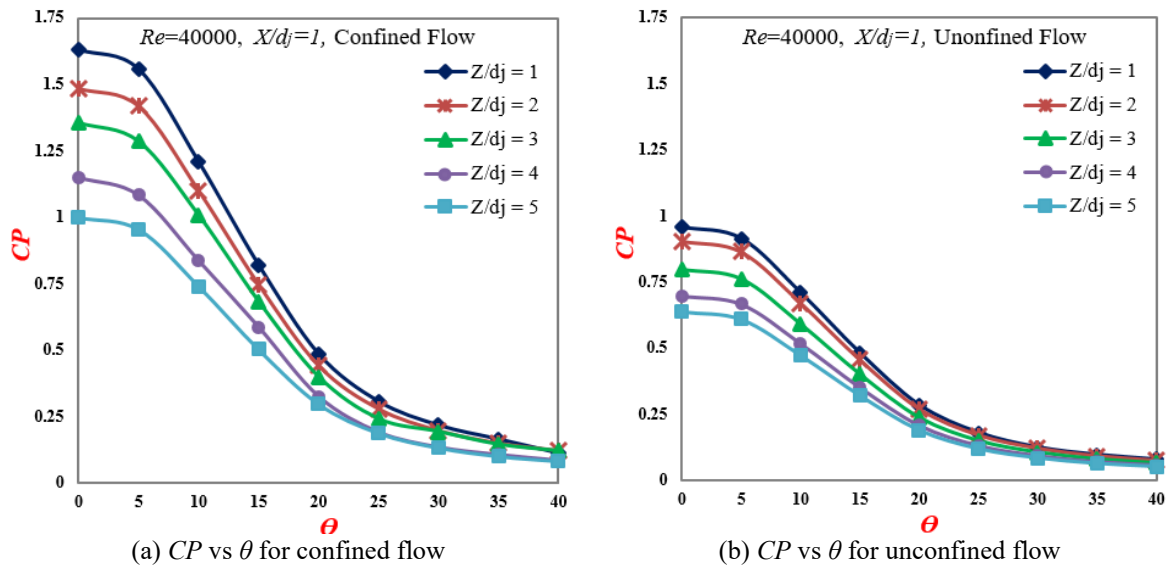
Figure 6. Variation of wall static pressure coefficient with curvature at various orifice exit-to-test element spacing.

(a) CP_O vs θ for confined flow   (b) CP_O vs θ for unconfined flow
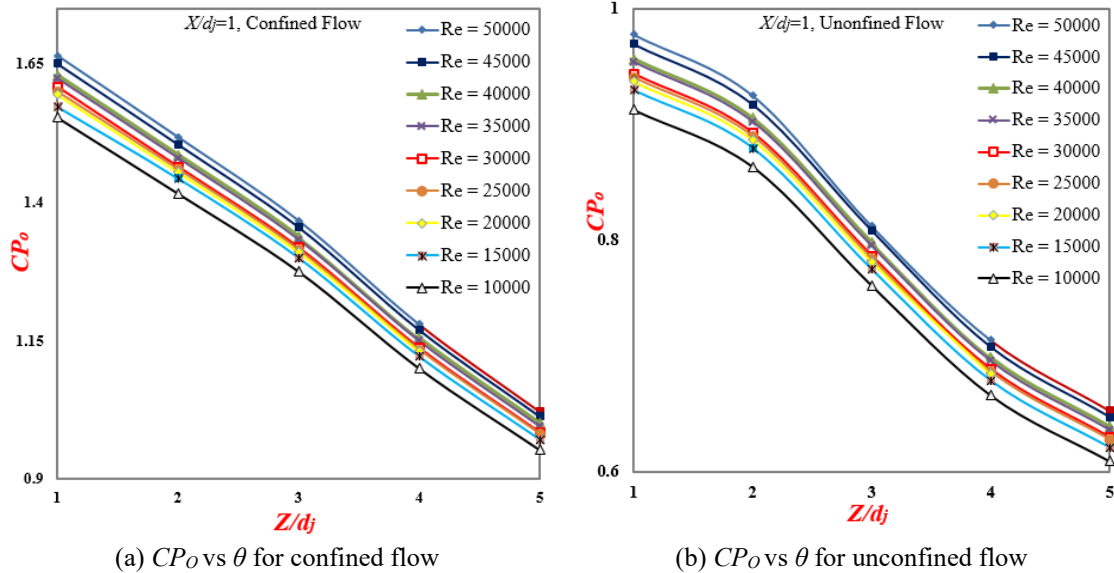
Figure 7. Variation of stagnation pressure coefficient with orifice exit-to-test surface spacing at various *Re*.

Influence of *Lateral Distance* on Pressure Coefficient.

The analysis is also carried from the obtained experimental results to understand the effect of the lateral or axial position of the jet (X/d_j) on the distribution of *CP* on a test plate in the spanwise direction. Figure 8 shows variation of *CP* at various X/d_j ranging from 0 to 5 at Z/d_j = 1 to 5 for both confined and unconfined condition at *Re* = 40000. From Figure 8, it is noted that the *CP* magnitudes are much higher than unity at the impingement position for smaller $X/d_j = 0$ and a significant drop in the *CP* is observed with an increase in the X/d_j ratio. The minimum *CP* identified at $X/d_j = 5$, that is with an increase in the X/d_j around 29% to 34%, drop in the *CP* observed. This phenomenon is mainly due to the shifting of jet streamline from the plate centreline; as result entrainment of surrounding air reduces jet strength at a particular position. Therefore from the analysis, it is understood that for lower X/d_j, higher *CP* and *CPo* values are observed for all examined flow parameters.

(a) *CP* vs X/d_j for confined flow   (b) *CP* vs X/d_j for unconfined flow
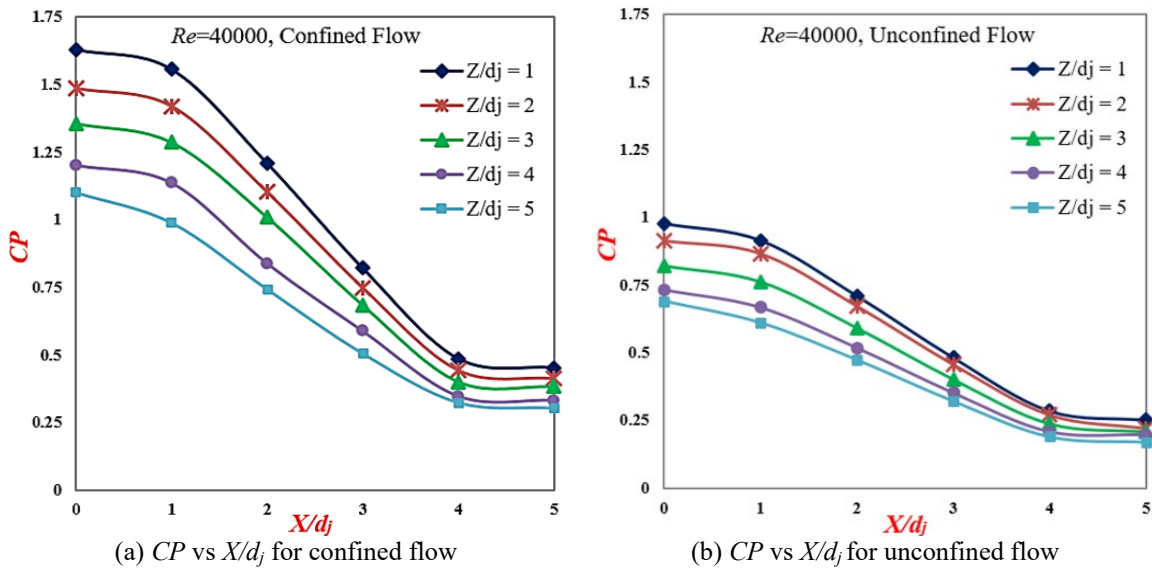
Figure 8. Variation of wall static pressure coefficient with curvature at a various lateral distance.

Comparison of Wall Static Pressure for Confined and Unconfined Flow

The confinement or flow restriction on the test element is another key parameter, which influences the *CP* and *CPo* distribution. From literature, it is noted the most of the studies on jet impingement are related to conventional circular jet for the unconfined condition. In the present study, the influence of confinement on *CP* and *CPo* distribution is identified experimentally. The confinement arrangement provides a well-defined path and restricts a jet within a potential core region, as shown in Figure 3. In Figure 9, graph (a) and (b) shows static pressure (*CP*) comparison, and graph (c) and (d) show the stagnation pressure (*CPo*) comparison for confined and unconfined conditions. From the obtained experimental data, around 41% to 56.6% in static pressure coefficients and around 48.5% to 58.8% in stagnation pressure coefficients enhancement is observed for confined flow condition. This remarkable change is noted in the distribution of *CP* and *CPo*,

as the confinement provides restriction to the jet to flow in a constrained path, which leads to the formation of a recirculation zone within the effective confinement zone. This recirculation gives a boost to jet by enhancing its kinetic energy as a result of high magnitude CP and CPo seen for a confined flow. The use of confinement gives enhancement in the CP and CPo by 48 % to 58 %. This data support the evidence of a recirculation region. Therefore from the obtained experimental results, the analysis shows that for all examined flow parameters the use of confinement in the jet impingement studies has a significant impact on the static pressure coefficients CP and CPo on flat test surface.

(a) CP vs θ at $Z/d_j = 1$ and $Re = 40000$

(b) CP vs θ at $Z/d_j = 4$ and $Re = 40000$

(c) CP_O vs Z/d_j at $X/d_j = 1$ & $Re = 40000$

(d) CP_O vs Z/d_j at $X/d_j = 1$ & $Re = 10000$
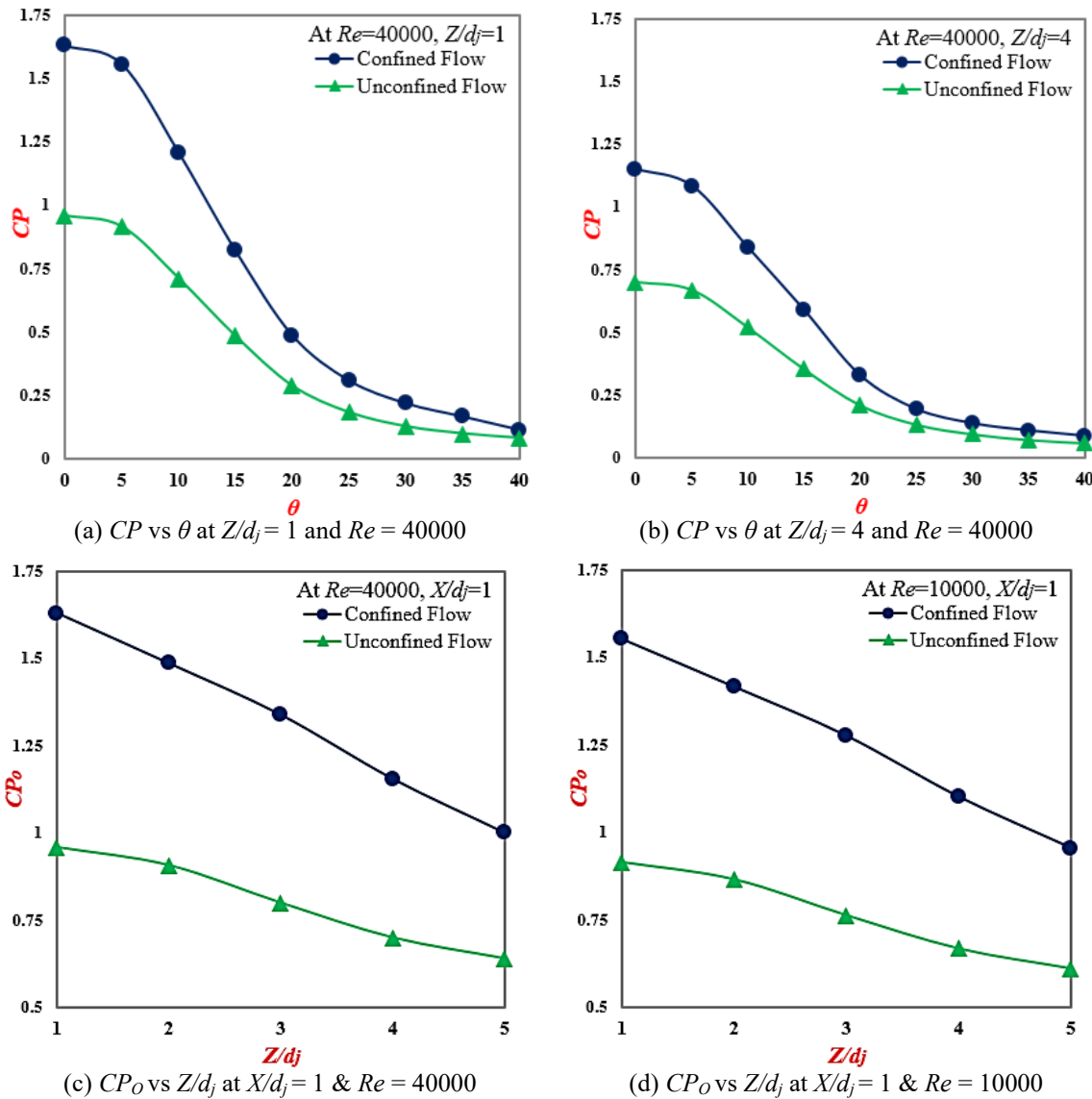
Figure 9. Comparison of wall pressure coefficient for confined and unconfined flow.

Pressure Loss Coefficient Analysis

Figure 10 gives the pressure loss coefficient (P_C) variation with orifice exit to rectangular plate distances ($Z/d_j = 1$ to 5) for $Re = 50000$ to 25000. The pressure loss coefficients are identified to know the pumping power for the jet. To measure pressure loss coefficients, a same experimental set up shown in Figure 1 was used with some minor modifications by attaching an additional pressure tap just before the jet exit. From the results, it is observed that the significant drop in pressure loss coefficients magnitude from Z/d_j 1 to 2 and with further increase in the Z/d_j 3 to 5 approximately, a constant value of P_C is seen. A higher value of P_{LC} is seen for confined flow when compared with the unconfined flow for all examined jet Reynold number. This result indicates that high pumping power is required in the confined flow. Similar contributions are observed for circular, square, rectangular and triangular orifice in early studies [23].

(a) P_C vs Z/d_j for confined flow   (b) P_C vs Z/d_j for unconfined flow
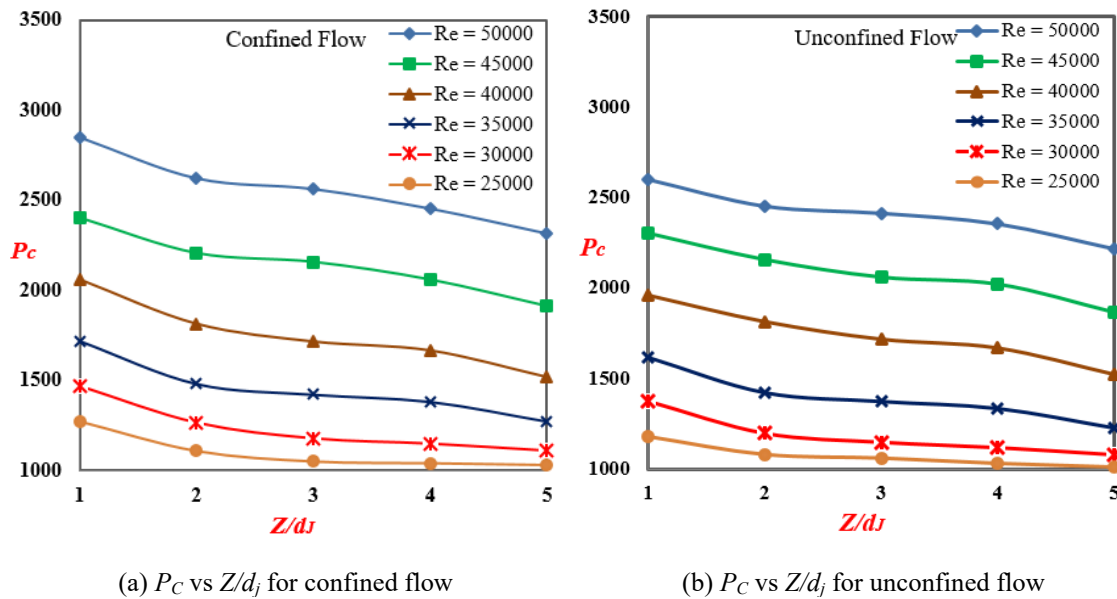
Figure 10. Variation of pressure loss coefficient (P_C) with orifice exit-to-plate distances at various *Re*.

CONCLUSION

In the present study, the wall pressure distribution (*CP* and *CPo*) on a rectangular element by impinging turbulent air jet from hexagonal orifice for a confined and unconfined condition is investigated experimentally under steady-state condition. Parametric studies were conducted for various jet Reynolds number (of *Re*=10000 to 50000) based on the hydraulic diameter of a hexagonal orifice; the Z/d_j is varied from 1 to 5 and X/d_j is varied from 0 to 5. The study shows that the use of confinement duct gives an interesting jet flow on the test surface and has a significant effect on both the static and stagnation pressure coefficients, and apart from confinement effect, the influence of orifice to test surface distance on wall pressure coefficients are identified. The key findings from the study are highlighted below, where the outcomes play a remarkable role in the heat transfer and fluid flow analysis in jet impingement studies.

i. The wall pressure coefficients *CP* and *CPo* show independent behaviour for the examined jet Reynold number *Re*= 10000-50000 in confined and unconfined flow condition for all Z/d_j = 1 to 5 and X/d_j= 0 to 5.

ii. The wall pressure coefficients *CP* and *CPo* magnitudes are high for lower orifice exit-to-test element distance (Z/d_j=1), and with the increase in the Z/d_j a remarkable drop in *CP* and *CPo* are noted for both confined and unconfined conditions. With the increase in the Z/d_j, around 32% to 37%, drop in *CP* and *CPo* are observed.

iii. The peak value of *CP* is observed at X/d_j = 0, and a remarkable drop in *CP* is noticed with an increase in X/d_j at all *Re* and with an increase in the X/d_j around 29% to 34% drop in the *CP* observed for both confined and unconfined condition.

iv. The wall static pressure *CP* for confined and unconfined conditions on a rectangular plate is consistent up to $\theta = 12^\circ$ and an appreciable drop in *CP* is noticed with an increase in θ. The peak value of *CP* is observed at $\theta = 0^\circ$ for all *Re* and Z/d_j.

v. The potential core of jet is observed for the Z/d_j ratio between 1 to 2 and X/d_j ratio between 0 to 2 as the velocity decay are minimum in these ranges.

vi. The use of confinement arrangement enhanced contribution of *CP* and *CPo* by 48% to 58% when compared to unconfined flow condition.

vii. The pressure loss coefficient (P_C) decreases with an increase in the jet to plate distance for both confined and unconfined flow conditions at all examined jet Reynold number. The pressure loss coefficient (P_C) are high for confined flow for all examined *Re*.

REFERENCES

[1] Lee S, Lee J, Lee D. Local heat transfer measurements from an elliptic jet impinging on a flat plate using liquid crystal. International Journal of Heat and Mass Transfer 1994; 37(6): 967-976.

[2] Martin H. Heat and mass transfer between impinging gas jets and solid surfaces. Advance in Heat Transfer 1977; 13: 1-60.

[3] Downs SJ, James EH. Jet impingement heat transfer - A literature survey. In: 24th National Heat Transfer Conference and Exhibition, Pennsylvania, USA; 9-12 August, 1987.

[4] Jambunathan K, Lai E, Moss MA, Button BL. A review of heat transfer data for single circular jet impingement, International Journal of Heat Fluid Flow 1992; 13 (2): 106–115.

[5] Viskanta R. Heat transfer to impinging isothermal gas and flame jets. Experimental Thermal Fluid Science 1993; 6 (2): 111-134.

[6]   Mujumdar K, Ranade V. Simulation of rotary cement kiln using a one dimensional model. Chemical Engineering Research and Design 2006; 84 (3): 165-177.

[7]   Lee S, Lee J, Lee D. Local heat transfer measurements from an elliptic jet impinging on a flat plate using liquid crystal. International Journal of Heat and Mass Transfer 1994; 37(6): 967-976.

[8]   Brignoni LA, Garimella SV. Effects of nozzle-inlet chamfering on pressure drop and heat transfer in confined air jet impingement, International Journal of Heat Mass Transfer 2000; 43 (7): 1133-1139.

[9]   Lee J, Lee S. The effect of nozzle aspect ratio on stagnation region heat transfer characteristics of elliptic impingement jet. International Journal of Heat and Mass Transfer 2000; 43(4): 555-575.

[10]   Gulati P, Katti V, Prabhu SV. Influence of the shape of the nozzle on local heat transfer distribution between smooth flat surface and impinging air jet. International Journal of Thermal Sciences 2009; 48(3): 602-617.

[11]   Kanamori A, Hiwada M, Oyakawa K, Senaha I. Effect of orifice shape on flow behavior and impingement heat transfer. The Open Transport Phenomena Journal 2011; 3: 9-16.

[12]   Singh D, Premachandran B, Kohli S. Effect of nozzle shape on jet impingement heat transfer from a circular Cylinder. International Journal of Thermal Sciences 2015; 96: 45-69.

[13]   Trinh XT, Fénot M, Dorignac E. The effect of nozzle geometry on local convective heat transfer to unconfined impinging air jets. Experimental Thermal and Fluid Science 2016; 70: 1-16.

[14]   Reodikar SA, Meena HC, Vinze R, Prabhu SV. Influence of the orifice shape on the local heat transfer distribution and axis switching by compressible jets impinging on flat surface. International Journal of Thermal Sciences 2016; 104: 208-224.

[15]   Meena HC, Reodikar SA, Vinze R, SV Prabhu. Influence of the shape of the orifice on the local heat transfer distribution between smooth flat surface and impinging incompressible air jet. Experimental Thermal and Fluid Science 2016; 70: 292-306.

[16]   Guo T, Rau MJ, Vlachos PP, Garimella SV. Axisymmetric wall jet development in confined jet impingement. Physics of Fluids 2017; 29: 025102.

[17]   Attala M, Maghrabie HM, Qauyum A, Al-Hasnawi AG, Specht E. Influence of the nozzle shape on heat transfer uniformity for in-line array of impinging air jets. Applied Thermal Engineering 2017; 120: 160-169.

[18]   Muvvala P, Balaji C, Venkateshan SP. Experimental investigation on heat transfer from square jets issuing from perforated nozzles, Heat Mass Transfer 2017; 53 (7): 2363-2375.

[19]   Long J, New TH. Vertical structures and behavior of an elliptic jet impinging upon a convex cylinder, Experimental Thermal and Fluid Science 2018; 100: 292-310.

[20]   Abraham S, Vedula RP. Local effectiveness and Nusselt number distributions for a rectangular jet impinging on a cylindrical convex surface at different angles. International Journal of Thermal Sciences 2018; 124: 407-422.

[21]   He C, Liu Y. Jet impingement heat transfer of a lobed nozzle: Measurements using temperature-sensitive paint and particle image velocimetry. International Journal of Heat and Fluid Flow 2018; 71: 111-126.

[22]   Singh A, BVSSS Prasad. Influence of novel equilaterally staggered jet impingement over a concave surface at fixed pumping power. Applied Thermal Engineering 2019; 148: 609-619.

[23]   Hanchinal AM, Katti VV. Effect of orifice geometry and orifice to test section spacing on distribution of wall static pressure on a convex surface. Journal of Mechanical Engineering and Sciences 2019; 13(2): 4835-4845.

[24]   Patil NG, Mujawar MA, Biradar SA, Adimurthy M, Katti VV. Influence of spent air confinement on pressure distribution over a flat plate impinged by an array of jets. International Journal of Ambient Energy. Epub ahead of print 20 January 2020. DOI: 10.1080/01430750.2020.1752798.

[25]   Hanchinal AM, Katti VV. Impingement of coaxial jet on convex element for confined and unconfined flow. Journal of Mechanical Engineering and Sciences 2020; 14(2): 6652-6662.

[26]   Baydar E, Ozmen Y. An experimental investigation on flow structures of confined and unconfined impinging air jets. Heat Mass Transfer 2006; 42: 338 346.

[27]   Adimurthy M, Katti VV. Local distribution of wall static pressure and heat transfer on a smooth flat plate impinged by a slot air jet. Heat Mass Transfer 2016; 53: 611-623.

[28]   Kessel W. Measurement uncertainty according to ISO/BIPM-GUM. Thermochimica Acta 2000; 382(1): 1-16.

[29]   Moffat RJ. Describing the uncertainties in experimental results. Experimental Thermal and Fluid Science 1998; 1: 3-17.

[30]   Kline SJ, McKlintock FA. Describing uncertainties in single sample experiments. Mechanical Engineering 1953; 75(1): 3-8.